Chinese Chemical Letters 33 (2022) 1979–1982

Contents lists available at ScienceDirect

Chinese Chemical Letters

journal homepage: www.elsevier.com/locate/cclet

A microenvironment sensitive pillar[5]arene-based fluorescent probe for cell imaging and drug delivery

Qing Wang*, Jingwen Fan, Xiaoyan Bian, Hang Yao, Xiaohui Yuan, Ying Han, Chaoguo Yan*

School of Chemistry and Chemical Engineering, Yangzhou University, Yangzhou 225002, China

ARTICLE INFO

Article history:
Received 28 June 2021
Revised 12 October 2021
Accepted 15 October 2021
Available online 22 October 2021

Keywords:
Fluorescent probe
Intramolecular charge transfer
Pillar[5]arene
Cell imaging
Drug delivery

ABSTRACT

Dansylamide (DNSA) is a typical ICT probe that has a favorable serum albumin sensitivity. Inspired by this, we designed a microenvironment sensitive fluorescent probe 4C-G through introducing DNSA into pillar[5]arene. Unlike DNSA, 4C-G displayed differentiated sensitivity to multiple proteins, which was benefit from pillar[5]arene assisted the probe to form complexes with proteins. 4C-G could not only be applied in imaging of HepG2, but also act as a favorable drug carrier for regorafenib (REG) encapsulation. The 4C-G-REG complex would aggregate into high drug-loading fluorescent nanoparticles in a physiological environment (pH 7.4). Such nanoparticles exhibited pH-triggered enrichment ability, which rapidly enriched REG in the acidic environment (pH 6.0). Furthermore, the complexation between 4C-G and REG maintained the imaging property of the probe and the excellent anticancer activity of the drug on HepG2.

Intramolecular charge transfer (ICT) fluorescent probes have gained considerable research attention in protein detection because of their sensibility to serum albumins [1–3]. Especially because albuminuria is an important diagnostic index for the chronic kidney disease, scientists developed various ICT probes for high-sensitive detection of human serum albumin (HSA) in recent years [4–6]. We have previously discussed an important prerequisite for the recognition is the ICT probe form a stable complex with HSA [7]. Interestingly, this recognition has no specific requirement for the binding sites of the protein. Otherwise, Sudlow *et al.* could not prove HSA contains two specific and widely recognized binding sites in structure [8,9]. Moreover, serum albumins have no specific structure that can be uniquely recognized by ICT probe. Some ICT probes exhibited responsiveness to multiple proteins. For example, squaraine dyes exhibit sensitivities to porcine mucin, exhibit transferrin, fibrinogen, trypsin and pepsin [10]. 11-Dansylamino undecanoic acid (DAUDA) displays a favorable fluorescence response to human intestinal fatty acids binding protein (hIFABP) and cavity of potassium channel (KcsA) [11,12]. What these proteins have in common is their aromatic amino acids, which contribute to their ultraviolet fluorescence [13]. Therefore, if the ICT probe has an appropriate structure for complexing, it can be sensitive to any fluorescent protein in theory.

Cancer is a leading cause of morbidity and mortality worldwide [14]. For a long time, scientists have been trying to develop new strategies for more efficient cancer therapy [15–18]. Developing advanced theranostic systems to achieve personalized medicine is a widely recognized strategy [19,20]. By encapsulation of fluorescent dyes, scientists developed various novel fluorescent theranostic agents [21–23]. However, these theranostic systems suffer from the requirements of multiple components. Inspired by the ICT probe has favorable fluorescent protein sensitivity, we decided to design a new platform for theranostic applications with the expectation of taking full advantage of this property.

Pillar[5]arene is the fifth generation of macrocyclic molecule that can directly deliver some drugs [24,25]. Moreover, its easily functionalized structure and electron-rich cavity endow it with excellent tuning of host–guest binding property [26–29]. In the present work, we described a pillar[5]arene-based ICT probe 4C-G (Scheme 1). This probe displayed differentiated sensibility to multiple proteins and could be applied in imaging of HepG2. 4C-G also was favorable drug carrier for an anticancer drug regorafenib (REG) encapsulation. The 4C-G-REG complex would aggregate into fluorescent nanoparticles in aqueous solution. These nanoparticles not only displayed favorable imaging properties in living cells but also maintained the excellent antitumor activity of REG on HepG2 cells.

Dansylamide (DNSA) is a typical ICT probe that has a favorable serum albumin sensitivity (Fig. S1 in Supporting information) [9]. In the present work, a pillar[5]arene-based fluorescent probe 4C-G was designed and synthesized by introducing DNSA into pillar[5]arene (Scheme S1 and Figs. S2-S4 in Supporting information). Since the pillar[5]arene group could not be excited at 300 nm (Fig. S5 in Supporting information), the intrinsic fluorescence of 4C-G

* Corresponding authors.
E-mail addresses: qingwang@yzu.edu.cn (Q. Wang), cgyan@yzu.edu.cn (C. Yan).

https://doi.org/10.1016/j.cclet.2021.10.040
1001-8417/

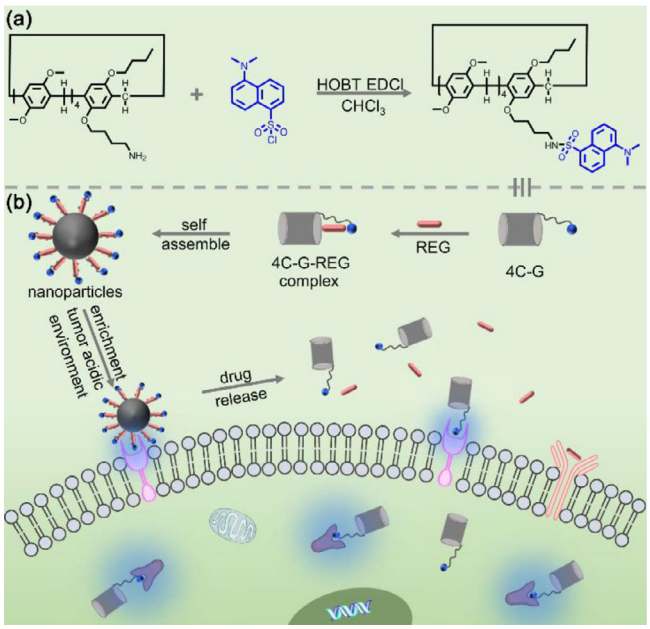

Scheme 1. Schematic illustration of (a) synthesis of 4C-G (b) the formation of fluorescent nanoparticles assembled by 4C-G-REG complex and their applications in cell imaging and drug delivery.

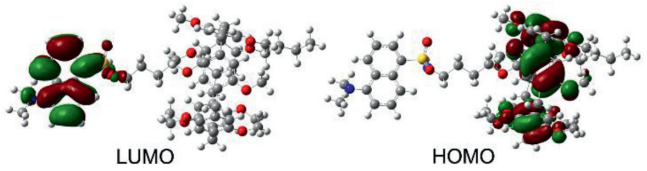

Fig. 1. HOMO-LUMO orbitals of 4C-G.

at λ_{ex} = 300 nm could fully be attributed to the DNSA group. Interestingly, different with DNSA, the emission maxima of 4C-G blue shifted approximately 55 nm. An apparent blue-shift could also be observed from the reactant dansyl chloride (DCL). Therefore, it was the slight difference in $-SO_2R$ result in their different fluorescence properties. Subsequently, the highest occupied molecular orbitals (HOMO) and the lowest unoccupied ones (LUMO) of 4C-G were obtained using the DFT/B3LYP/6-311G (d,p) method (Fig. 1). The HOMO was primarily localized on the pillar[5]arene group, whereas the LUMO was almost completely localized in the DNSA group, indicating the presence of the pillar[5]arene group evidently changed the electron density distribution of DNSA. The energy gap of 4C-G (ΔE = 3.108 eV) was weaker than that of DNSA (ΔE = 4.042 eV) and DCL (ΔE = 3.457 eV). But the presence of –Cl in DCL and the alkyl chain in 4C-G weakened the intramolecular charge transfer state of DNSA. So 4C-G and DCL exhibited stronger intrinsic fluorescence than DNSA (Fig. S6 in Supporting information). Nonetheless, the separated charge state still remained in 4C-G.

We then investigated the sensibility of 4C-G to various proteins, including α-lactalbumin, β-lactoglobulin, bovine serum albumin (BSA), HSA, lysozyme and trypsin (Fig. 2a and Fig. S7 in Supporting information). As expected, 4C-G inherited the favorable protein microenvironment-sensitive property of DNSA. However, unlike DNSA, 4C-G exhibited different sensitivities to multiple proteins, which were no longer limited to serum albumins. 4C-G had a broad protein sensitivity. Forming a complex is a prerequisite for an ICT probe to recognize protein. Since DNSA only had serum albumin sensitivity, the above phenomena could be attributed to pillar[5]arene assisted the DNSA group to form complexes with the proteins. The presence of pillar[5]arene in the structure improved the insertion of DNSA into various proteins, which endowed 4C-G with broad protein sensitivity. Moreover, 4C-G exhibited strong BSA sensitivity and weak trypsin sensitivity, indicating the difference in spatial structure influenced the responsiveness of 4C-G to the proteins. With the enhancement of 4C-G fluorescence (λ_{ex} = 280 nm), the intrinsic fluorescence of all proteins was quenched (Fig. S8 in Supporting information). Therefore, the fluorescence enhancement of 4C-G could not be simply attributed to the restriction on the freedom degree of the probe inside the proteins because the intrinsic fluorescence of proteins was also affected. We previously discussed the gallate esters should be formed electromagnetic coupling with the whole HSA and thus the probe could recognize HSA no matter whether the protein could be excited [7]. In the present work, similar luminescence phenomena also presented in the 4C-G-protein interaction. Given the differences in protein spatial structure, we believe that the differences of protein electromagnetic field leaded to the distinct responsiveness of 4C-G to various proteins.

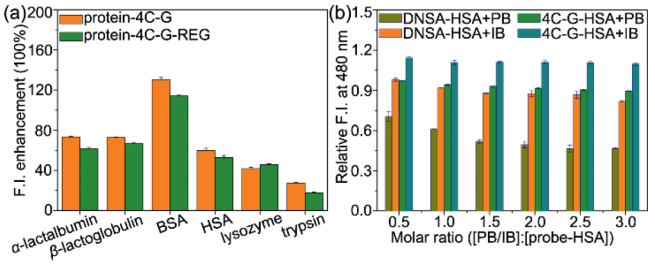

Fig. 2. (a) Fluorescence enhancement ratios of 4C-G in the presence of different proteins (λ_{ex} = 300 nm and λ_{em} = 480 nm). $C_{(4C\text{-}G)} = C_{(protein)}$ = 4.0 μmol/L. (b) Relative fluorescence intensities of DNSA–HSA complex and 4C-G–HSA complex (λ_{ex} = 300 nm and λ_{em} = 480 nm) with increasing molar equivalents of PB/IB from 0.5, 1.0, 1.5, 2.0, 2.5 to 3.0. $C_{(DNSA)} = C_{(4C\text{-}G)} = C_{(HSA)}$ = 4.0 μmol/L.

HSA has two primary hydrophobic binding sites for ligand binding (Site I and Site II) [30]. DNSA mainly binds to Site I while dansylsarcosine selectively bind to Site II [31]. In order to confirm whether 4C-G and DNSA share the same binding site in HSA, displacement experiments were then performed. Phenylbutazone (PB) and ibuprofen (IB) were selected as competitive ligands because they have no ICT probe characteristic and specifically bind to Site I and Site II, respectively. As shown in Fig. 2b, the addition of IB to the 4C-G-HSA mixture promoted the fluorescence of the probe further enhanced, indicating 4C-G shared a different binding site with IB. Meanwhile, the addition of PB slightly suppressed the enhanced fluorescence of 4C-G, whereas the suppression was significantly weaker than that to DNSA. Therefore, 4C-G did not completely embedded into site I but bound around to the site. This binding pose did not benefit the electromagnetic coupling between 4C-G and HSA, and thus 4C-G exhibited weak HSA sensitivity.

Subsequently, we evaluated the possibility of 4C-G as drug carrier for REG encapsulation. The anti-cancer drug REG (Stivarga®), a multikinase and chaperone inhibit, has been approved for the treatment of metastatic colorectal cancer, gastrointestinal stromal tumours, and hepatocellular carcinoma [32,33]. Obvious downfield chemical shifts could be observed in partial protons of REG (*e.g.*, Hm and Hl) when in the presence of 4C-G as those protons suffered deshielding effect from the probe (Fig. 3). Moreover, the characteristic absorption peak of 4C-G at around 295 nm became apparently strong after adding REG to the solution (Fig. S9 in Supporting information). All these results indicated that 4C-G formed complex with REG in solution. Nuclear overhauser effect (NOE) correlative signals were observed between protons of sulfanilamide bond in 4C-G and protons of REG, suggesting REG was fixed at the molecular gap between pillar[5]arene group and DNSA group (Fig.

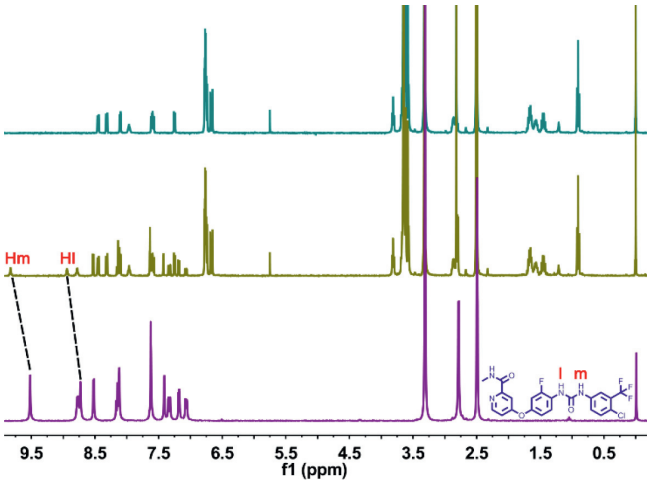

Fig. 3. ^{1}H NMR spectra (DMSO-d_6, 298 K) of 4C-G, REG and their complex. $C_{(4C\text{-}G)} = C_{(REG)} = 3.0$ mmol/L.

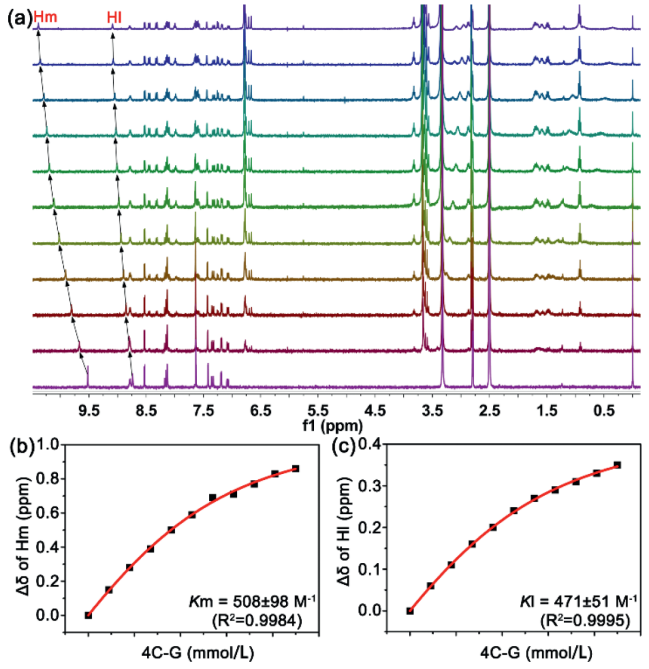

Fig. 4. (a) ^{1}H NMR spectra (DMSO-d_6, 298 K) of REG at a constant concentration of 5.0 mmol/L with different concentrations of 4C-G: 0, 0.9, 1.8, 2.7, 3.6, 4.5, 5.4, 6.3, 7.2, 8.1, 0.9 mmol/L. (b, c) The chemical shift changes of Hm and Hl on REG upon the addition of 4C-G.

S10 in Supporting information). Based on the ^{1}H NMR titration experiment (Fig. 4), the association constants of Hm and Hl with sulfanilamide bond were determined to be Km = 508 ± 98 L/mol and Kl = 471 ± 51 L/mol, respectively. Sulfanilamide bond played an important role in stabilizing 4C-G-REG complex. The binding stoichiometry between 4C-G and REG was then determined as approximately 1:1 using Job's plot method (Fig. S11 in Supporting information). Besides, we found the presence of REG had little effect on the fluorescence responsiveness of 4C-G to various proteins (Fig. 2a). The 4C-G-REG complex still has a favorable protein-microenvironment sensitive property.

By utilizing the complexation of REG with 4C-G, we further obtained their high-order aggregates in aqueous solution. The 4C-G-REG complex (ratio of [4C-G]/[REG] = 1:1) in ethanol were injected into ultrapure water under stirring, and the unaggregated components in the sample (50 μmol/L, containing 2% ethanol) were

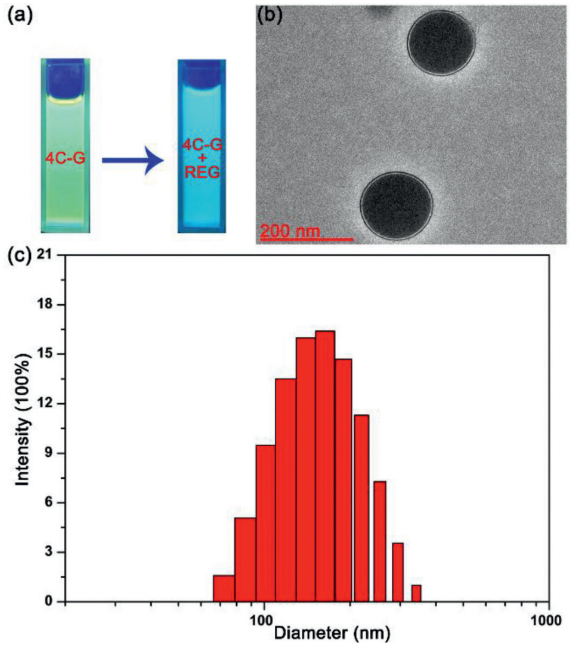

Fig. 5. (a) Photographs of 4C-G and 4C-G-REG complex aggregates in physiological environment (pH 7.4) under a UV-lamp (365 nm). (b) TEM image of 4C-G-REG complex aggregates. (c) DLS data of 4C-G-REG complex aggregates.

removed by dialysis (molecular weight cutoff 8000) against 0.01 mol/L of PBS (pH 7.4). As shown in Fig. S12a (Supporting information), a clear Tyndall effect was observed in the aqueous solution. The 4C-G-REG complex were gathered to form well-defined nanoparticles with an average diameter of 149.6 nm in the solution (Fig. 5). According to the reported method in literature [34], HPLC was used to measure the mass of REG loaded into the nanoparticles (Fig. S13 in Supporting information). By using the following equation: $EE(\%) = (m_{REG\text{-}loaded}/m_{REG}) \times 100\%$, the maximal REG encapsulation efficiency of the 4C-G-REG nanoparticles was calculated to be 89.2%. 4C-G exhibited high drug-loading capacity. Such nanoparticles had good stability in physiological environment (pH 7.4, ζ-potential = −23.3 mV). Nevertheless, the 4C-G-REG nanoparticles were easily aggregated into larger particles and rapidly precipitated from acid environment (pH 6.0, Fig. S12b in Supporting information), displaying pH-trigged enrichment ability. This phenomenon may be attributed to the interaction of alkaline REG with 4C-G was weakened in acidic environment, and thus the insoluble drug was rapidly released in large quantities from the 4C-G-REG complex. Considering that the tumor environment is acidic, the 4C-G-REG nanoparticles, with good pH-responsiveness and stability, can potentially be applied for tumor acidic microenvironment targeting.

The cytotoxicities of REG, 4C-G and 4C-G-REG complex were evaluated by using a CCK-8 assay in HepG2 cells (Fig. 6). REG exhibited favorable anticancer activity. More than 94.5% of cells were still viable with 4C-G for 24 h in different concentrations, demonstrating that 4C-G had low cytotoxicity. The 4C-G-REG complex also evidently reduced the cell viability of HepG2. But, interestingly, the anticancer activity displayed by 4C-G-REG complex was comparable to that exhibited by free REG, suggesting the complex maintained the excellent anticancer activity of the drug.

The potential application of 4C-G in live-cell imaging was investigated by incubating HepG2 cells with 4C-G (8 μmol/L) for 4 h at 37 °C. Evident blue fluorescence was observed in HepG2 cells upon excitation at 345 nm (Fig. 7). Like many ICT probes [35,36], 4C-G evenly distributed in the membrane and cytoplasm of HepG2 cells. 4C-G could be applied for cell imaging. Moreover, intense blue flu-

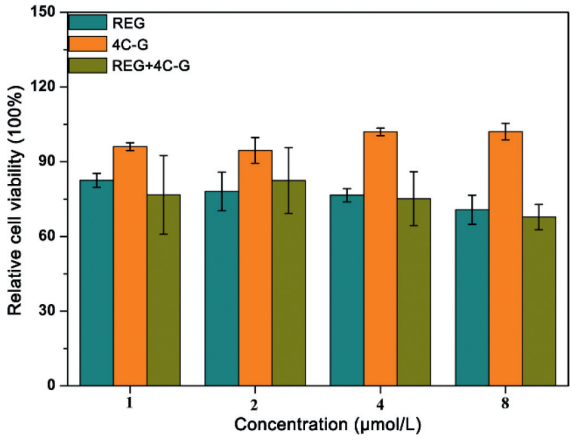

Fig. 6. *In vitro* cytotoxicities of 4C-G, REG and 4C-G-REG complex against HepG2 cells after 24 h of incubation.

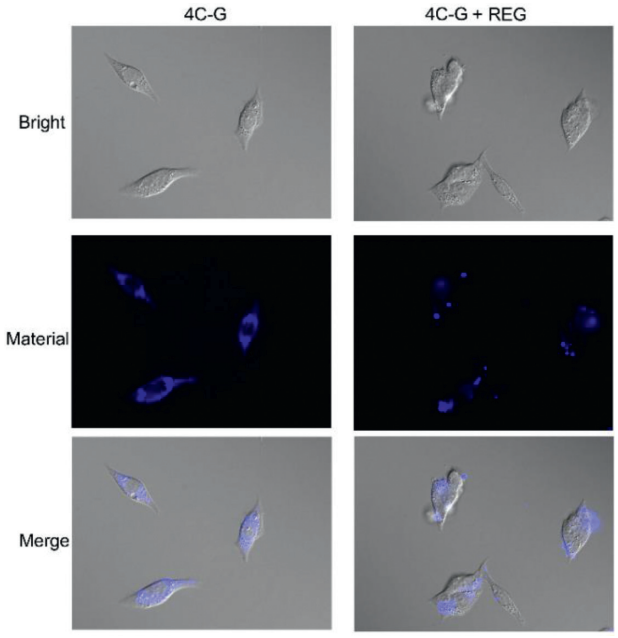

Fig. 7. Fluorescent imaging of HepG2 cells incubated with 4C-G and 4C-G-REG complex for 4 h at 37 °C. $C_{(4C\text{-}G)} = C_{(REG)} = 8.0$ μmol/L.

orescence emission still could be observed when the cells were incubated with 4C-G-REG complex, implying the complexation of 4C-G with REG retained the favorable imaging property of the probe.

In summary, we designed and synthesized a protein microenvironment-sensitive probe (4C-G) based on intramolecular charge transfer mechanism. Different with DNSA, 4C-G displayed favorable sensitivity to multiple proteins, especially to BSA. The presence of pillar[5]arene in the structure improved the insertion of DNSA into various proteins, which endowed 4C-G with broad protein sensitivity. Benefit from its favorable fluorescence responsiveness, 4C-G exhibited an excellent living-cell imaging property. As a pillar[5]arene-based probe, 4C-G also displayed a favorable encapsulation property for REG. Surprisingly, the complexation between 4C-G and REG maintained the live-cell imaging property of the probe and excellent anticancer activity of the drug, which showed high potential for cancer theranostic applications.

Declaration of competing interest

The authors declare that they have no known competing financial interests or personal relationships that could have appeared to influence the work reported in this paper.

Acknowledgments

This work was supported by the Scientific Research Staring Foundation of Yangzhou University, Yangzhou Green Yang Gold Phoenix plans and Jiangsu Shuangchuang Project.

Supplementary materials

Supplementary material associated with this article can be found, in the online version, at doi:10.1016/j.cclet.2021.10.040.

References

[1] J. Chen, Y.W. Li, X.K. Feng, et al., Spectrochim. Acta A 246 (2021) 119041.
[2] V.S.D. Gomes, H.M.R. Gonçalves, R.E.F. Boto, P. Almeida, L.V. Reis, J. Photoch. Photobio. A 400 (2020) 112710.
[3] X.S. Li, S. Yu, Y. Lee, et al., J. Am. Chem. Soc. 141 (2019) 1366–1372.
[4] C. Chen, Y.H. Yao, W.S. Wang, et al., Spectrochim. Acta A 241 (2020) 118685.
[5] Y. Kim, E. Shin, W. Jung, M.K. Kim, Y. Chong, Sensors 20 (2020) 1232.
[6] Z.Q. Liang, Y.Q. Sun, H.J. Zeng, et al., Anal. Chem. 92 (2020) 16130–16137.
[7] Q. Wang, X.Y. Bian, Z.L. Suo, et al., J. Lumin. 213 (2019) 530–537.
[8] G. Sudlow, D.J. Birkett, D.N. Wade, Mol. Pharmacol. 11 (1975) 824–832.
[9] G. Sudlow, D.J. Birkett, D.N. Wade, Mol. Pharmacol. 12 (1976) 1052–1061.
[10] C. Butnarasu, N. Barbero, C. Barolo, S. Visentin, Dyes Pigm. 184 (2021) 108873.
[11] N. Smithers, J.H. Bolivar, A.G. Lee, J.M. East, Biochemistry 51 (2012) 7996–8002.
[12] R. Patil, A. Laguerre, J. Wielens, et al., ACS Chem. Biol. 9 (2014) 2526–2534.
[13] J.R. Lakowicz, Principles of Fluorescence Spectroscopy, 3rd Edition, Springer, 2006.
[14] R.L. Siegel, K.D. Miller, A. Jemal, CA Cancer J. Clin. 70 (2020) 7–30.
[15] M. Dimri, A. Satyanarayana, Cancers 12 (2020) 491.
[16] Q. Cheng, S.K. Li, Y.L. Ma, H. Yin, R.B. Wang, Chin. Chem. Lett. 31 (2020) 1235–1238.
[17] S.K. Li, Y. Gao, Y.F. Ding, A.N. Xu, H.P. Tian, Chin. Chem. Lett. 32 (2021) 313–318.
[18] J. Yang, D.H. Dai, L.J. Ma, Y.W. Yang, Chin. Chem. Lett. 32 (2021) 729–734.
[19] B. Jamil, Nanotheranostics: Applications and Limitations, Springer, 2019.
[20] Y.X. Chen, B.W. Li, X.H. Chen, et al., Chin. Chem. Lett. 31 (2020) 1153–1158.
[21] W.W. Mu, D.D. Jiang, S.J. Mu, et al., ACS Appl. Mater. Inter. 11 (2019) 23591–23604.
[22] Y. Zhang, S. Uthaman, W. Song, et al., ACS Biomater. Sci. Eng. 6 (2020) 5012–5023.
[23] J.W. Cui, Z.L. Gao, W.W. Mu, et al., J. Mater. Chem. B 8 (2020) 6866–6876.
[24] Z.H. Qi, K. Achazi, R. Haag, et al., Chem. Commun. 51 (2015) 10326–10329.
[25] T. Ogoshi, T. Kakuta, T. Yamagishi, Angew. Chem. Int. Ed. 58 (2019) 2197–2206.
[26] P.Y. Lia, Y. Chen, Y. Liu, Chin. Chem. Lett. 30 (2019) 1190–1197.
[27] Y.M. Chen, S.Y. Sun, D. Lu, Y.J. Shi, Y. Yao, Chin. Chem. Lett. 30 (2019) 37–43.
[28] Q. Wang, X.Y. Bian, X.L. Chen, Y. Han, C.G. Yan, J. Mol. Struct. 1210 (2020) 128004.
[29] H. Guo, X. Yan, B. Lu, et al., J. Mater. Chem. C 8 (2020) 15622–15625.
[30] K. Yamasaki, V.T.G. Chuang, T. Maruyama, M. Otagiri, BBA-Gen Subjects 1830 (2013) 5435–5443.
[31] A.J. Ryan, J. Ghuman, P.A. Zunszain, C.W. Chung, S. Curry, J. Struct. Biol. 174 (2011) 84–91.
[32] G. Lombardi, G.L. De Salvo, A.A. Brandes, et al., Lancet Oncol 20 (2019) 110–119.
[33] B. Wang, F. Wang, A. Ding, H. Zhao, X. Bu, Clin. Transl. Oncol. 22 (2020) 1491–1498.
[34] K. Fujita, M. Miura, H. Shibata, Biomed. Chromatogr. 30 (2016) 1611–1617.
[35] X. Pang, Y.Q. Li, Q.J. Lu, et al., Analyst 146 (2021) 521–528.
[36] X.F. Hou, Z.S. Li, Y.Q. Li, et al., Spectrochim. Acta A 246 (2021) 119030.